Research article

Hamed Dalir[a,*], Farzad Mokhtari-Koushyar[a], Iman Zand[a], Elham Heidari[a], Xiaochuan Xu, Zeyu Pan, Shuai Sun, Rubab Amin, Volker J. Sorger and Ray T. Chen*

Atto-Joule, high-speed, low-loss plasmonic modulator based on adiabatic coupled waveguides

https://doi.org/10.1515/nanoph-2017-0092
Received September 18, 2017; revised February 22, 2018; accepted February 23, 2018

Abstract: In atomic multi-level systems, adiabatic elimination (AE) is a method used to minimize complicity of the system by eliminating irrelevant and strongly coupled levels by detuning them from one another. Such a three-level system, for instance, can be mapped onto physically in the form of a three-waveguide system. Actively detuning the coupling strength between the respective waveguide modes allows modulating light to propagate through the device, as proposed here. The outer waveguides act as an effective two-photonic-mode system similar to ground and excited states of a three-level atomic system, while the center waveguide is partially plasmonic. In AE regime, the amplitude of the middle waveguide oscillates much faster when compared to the outer waveguides leading to a vanishing field build up. As a result, the plasmonic intermediate waveguide becomes a "dark state," hence nearly zero decibel insertion loss is expected with modulation depth (extinction ratio) exceeding 25 dB. Here, the modulation mechanism relies on switching this waveguide system from a critical coupling regime to AE condition via electrostatically tuning the free-carrier concentration and hence the optical index of a thin indium thin oxide (ITO) layer resides in the plasmonic center waveguide. This alters the effective coupling length and the phase mismatching condition thus modulating in each of its outer waveguides. Our results also promise a power consumption as low as 49.74 aJ/bit. Besides, we expected a modulation speed of 160 GHz reaching to millimeter wave range applications. Such anticipated performance is a direct result of both the unity-strong tunability of the plasmonic optical mode in conjunction with utilizing ultra-sensitive modal coupling between the critically coupled and the AE regimes. When taken together, this new class of modulators paves the way for next generation both for energy and speed conscience optical short-reach communication such as those found in interconnects.

Keywords: indium thin-oxide; plasmonics; atto-Joule optoelectronics; adiabatic elimination; subwavelength spacing; optical modulator.

1 Introduction

Future high-performance, multi-core, parallel computing systems require a radical approach to provide power-efficient and ultra-dense high-speed interconnects at a low cost. Silicon-based optical modulators are one of the key components in this value proposition because of its low cost, latency, and power consumption [1, 2]. For photonic solutions to become competitive in intra- or inter-chip applications, the communication link power consumption, including optical modulators, must be scaled down from ~10 pJ/bit at present to ≲1 fJ/bit in the next few years, and likely to ≲100 aJ/bit in the mid-term. Recently, Intel has acknowledged that the future of integrated optical circuit relies on technologies that aggressively reduce power consumption with their reasonable performance (https://www.extremetech.com/extreme/222590-an-end-to-scaling-intels-next-generation-chips-will-sacrifice-speed-to-reduce-power). As of today, two types of optical

[a]**Hamed Dalir, Farzad Mokhtari-Koushyar, Iman Zand and Elham Heidari:** These authors contributed equally to this work.
***Corresponding authors: Hamed Dalir,** Omega Optics, Inc., 8500 Shoal Creek Blvd., Building 4, Suite 200, Austin, TX 78757, USA, e-mail: hamed.dalir@omegaoptics.com; and **Ray T. Chen,** Department of Electrical and Computer Engineering, The University of Texas at Austin, 10100 Burnet Rd., MER 160, Austin, TX 78758, USA, e-mail: chenrt@austin.utexas.edu
Farzad Mokhtari-Koushyar, Elham Heidari and Zeyu Pan: Department of Electrical and Computer Engineering, The University of Texas at Austin, 10100 Burnet Rd., MER 160, Austin, TX 78758, USA
Iman Zand: Hub Petroleum, 1100 Poydras Street, Suite 2925, New Orleans, LA 70163, USA
Xiaochuan Xu: Omega Optics, Inc., 8500 Shoal Creek Blvd., Building 4, Suite 200, Austin, TX 78757, USA
Shuai Sun, Rubab Amin and Volker J. Sorger: Department of Electrical and Computer Engineering, George Washington University, 800 22nd Street, Science and Engineering Hall, Washington, DC 20052, USA

modulators (refractive- or absorptive-based) are available. For the refractive approach, changing the plasma dispersion effect or free carrier absorption in silicon manipulates the real part of material permittivity and hence the modulation occurs. Nevertheless, because of a small change in the real part of material permittivity, modulators such as Mach-Zehnder's demand several hundreds of micrometers to acquire sufficient extinction ratios required to achieve the desired bit-error-rate of the signal. This results in a large footprint, low operation speed and eventually large power consumption modulators [3, 4]. To overcome these limits, other refractive modulators are operated with multiple-pass but in single-beam interference, such as disk or ring resonator-based devices. Due to the nature of the resonance, a narrowband modulation of 0.1 nm with a stringent fabrication process is expected [5, 6]. In addition, a precise temperature stabilization to hold the device on resonance is indispensable, requiring high static power consumption [7]. On the contrary, absorptive-based modulators manipulate the transmission intensity directly, that is without the need for interference, by means of modifying the imaginary part of the material permittivity such as saturable absorption, electro-absorption, the Franz-Keldysh effect (FKE), and the quantum-confined Stark effect [8–10]. Germanium modulators (FKE-based) offer a relatively high-speed operation but suffer from a large insertion loss related to the intrinsic Ge Si absorption loss at zero bias voltage [8–10]. Furthermore, complementary metal–oxide–semiconductor (CMOS)-compatible integration comes with stringent process requirements such as those found in epitaxial growth, wafer- or die-bonding, which limits the liability of the final devices [8–10]. Recently, optical modulators based on two-dimensional (2D) materials such as graphene devices provide advantages of compact footprint and ultrafast modulation speed across a broad range of wavelengths [7, 11, 12]. Nevertheless, because of the poor overlapping of light with the thin 2D absorber, relatively large biasing voltage is required to attain modulation [12]. Previously, we have experimentally demonstrated a novel plasmonic modulator based on a thin layer of ITO with 1 dB per micrometer modulation strength, while showing improvement over graphene devices, this concept limits modulation speeds beyond 100 GHz with sub-volt operation at reasonable low insertion loss (<10 dB) [13].

Here, we proposed an atto-Joule, low-loss, and high-speed plasmonic optical modulator based on tunability of three adiabatically coupled waveguides (ACW). Analogous to AE in an atomic three-level system, two outer waveguides function as ground and excited states, where the intermediate waveguide is equivalent to the "dark state" (effective two-level system). In atomic three-level systems, AE is a method that is used to minimize complicity of the system by eliminating irrelevant, strongly coupled nearby levels with a very large detuning between them. In this case, amplitude of the middle level oscillates much faster when compared to the other levels leading to no significant build up. As a result, the three-level system reduces to an effective two-level system with a vanishing coupling strength (i.e. diverging mode coupling length) between the ground and excited states, with the intermediate level becoming a "dark" state [14, 15]. The dark state, namely the middle waveguide has a plasmonic metal-oxide-semiconductor (MOS) configuration, which concentrates the optical modes' transverse magnetic (TM) field into a thin ITO layer, thus allowing for a high modal overlap enabling efficient tunability [16–18]. The modulation mechanism originates from electrically changing the free carrier concentration of the ITO layer that actively controls the effective coupling of the outer waveguides; consequently, the coupling strength and phase mismatching condition change and modulation take place. Our simulation results indicate that the proposed device will operate with a power consumption as low as 50 atto-Joule and exceed 25 dB extinction ratio. In addition, our

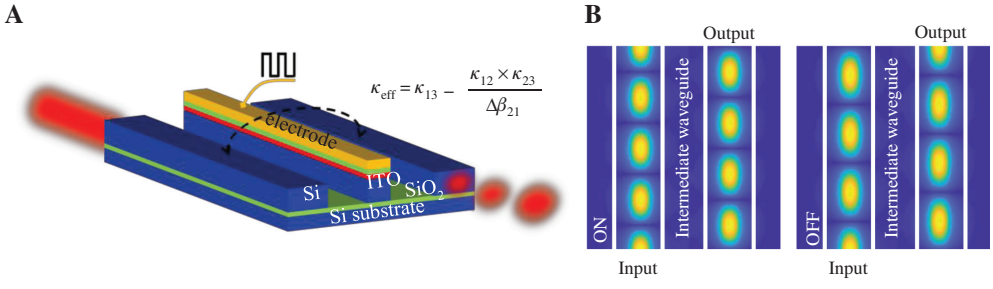

Figure 1: Adiabatic elimination in coupled waveguides with sub-wavelength spacing (λ/30).
(A) Schematic structure. (B) Fundamental transverse magnetic mode of the adiabatically coupled waveguides. Outer waveguides are identical with a width of 180 nm and middle waveguide is 80 nm, spacing of the outer waveguides to middle waveguides is 50 nm, the height of the waveguides is 550 nm.

ACW plasmonic modulator provides high-speed operation exceeding the millimeter wave range radio over fiber application whilst insertion loss is only 1.4 dB with 100 mV biased voltage. The proposed plasmonic device enables novel architectures for on-chip optical communications.

Our compact plasmonic modulator is composed of three-coupled waveguides, where the outer waveguides are made up of two identical silicon photonics strip waveguides (Figure 1). Intermediate waveguide consists of a metallic Au-pad with a gate oxide of 20 nm-thick SiO_2 and an active ITO with the thickness of 20 nm sandwiched between them. Here, coupling between the two outer waveguides becomes controllable through varying a bias voltage across the MOS capacitor in an intermediate waveguide. This leads to the mode's index change altering the propagation mismatch and hence the inversion length of the outer waveguides. The three coupled mode equations for this symmetric structure is written in Eq. (1) with $\Delta\beta_{21}=\beta_2-\beta_1$, where β_1 and β_2 are the propagation constants of the outer and middle waveguides, respectively [15]. κ_{13} is the coupling strength between the identical outer waveguides, while κ_{12} and κ_{21} are the coupling strengths between the un-identical outer and middle waveguides [19]. Due to the symmetry, $\kappa_{12}=\kappa_{32}$ and $\kappa_{21}=\kappa_{23}$. When $\kappa_{21} \ll |\Delta\beta_{12}|$, the AE condition is realized [14] and the effective coupling strength between the two outer waveguides is $\kappa_{\text{eff}}=\kappa_{13}-\kappa_{12}\kappa_{23}/\Delta\beta_{21}$ [14]. As shown in Figure 1B, the TM mode injected through one of the outer waveguides propagates merely in the other outer waveguide. This confirms the AE condition, where the center plasmonic waveguide is in the dark state. The outer waveguides are identical with a width of 180 nm, whereas the center waveguide is 80 nm wide, where the total gap between the outer waveguides is 180 nm (i.e. ~$\lambda/8$) with a height of 550 nm-thick silicon, while the general platform is silicon-on-insulator.

$$\frac{\mathrm{d}}{\mathrm{d}z}\begin{vmatrix}A_1\\A_2\\A_3\end{vmatrix}=j\begin{vmatrix}0 & \kappa_{12}\exp(j\Delta\beta_{21}z) & \kappa_{13}\\ \kappa_{21}\exp(-j\Delta\beta_{21}z) & 0 & \kappa_{23}\exp(-j\Delta\beta_{21}z)\\ \kappa_{13} & \kappa_{32}\exp(j\Delta\beta_{21}z) & 0\end{vmatrix}\cdot\begin{vmatrix}A_1\\A_2\\A_3\end{vmatrix} \quad (1)$$

Here, the loss and effective index of the optical modes are calculated via compact 2D finite-difference time domain method. Metallic boundary conditions are

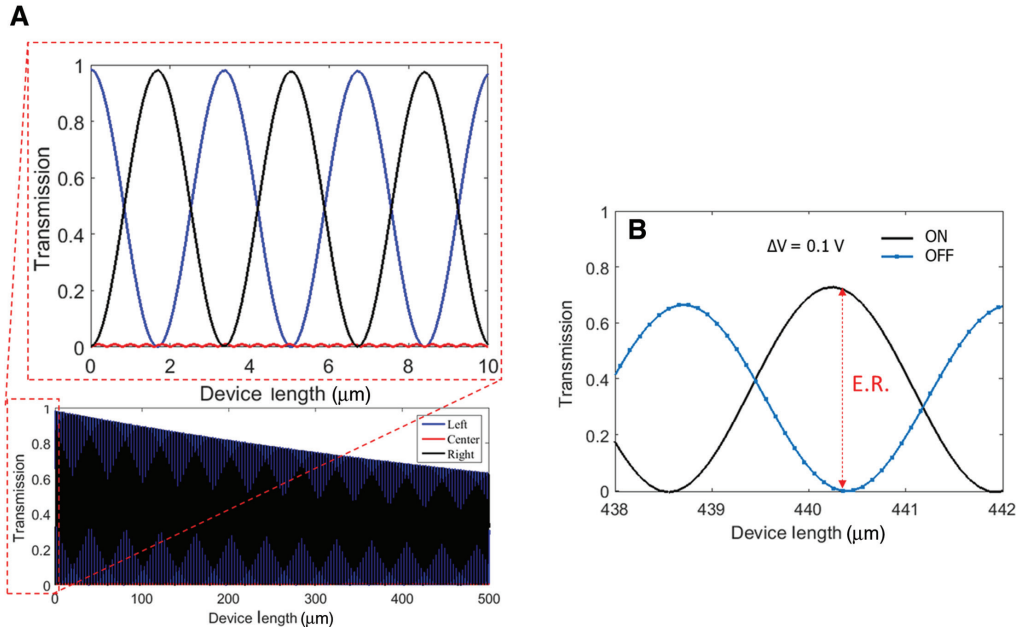

Figure 2: Atto-Joule modulation in adiabatic coupled waveguides.
(A) Effective coupling in three waveguides with adiabatic elimination approximation (as each of the two coupling processes is greatly detuned, the amplitude of the intermediate waveguide oscillates very fast in comparison to the slow varying population in the outer waveguides resulting in no significant build up and remains at its initial value). (B) Active coupling control between outer waveguides in adiabatic elimination configuration under 100 mV of driving voltage.

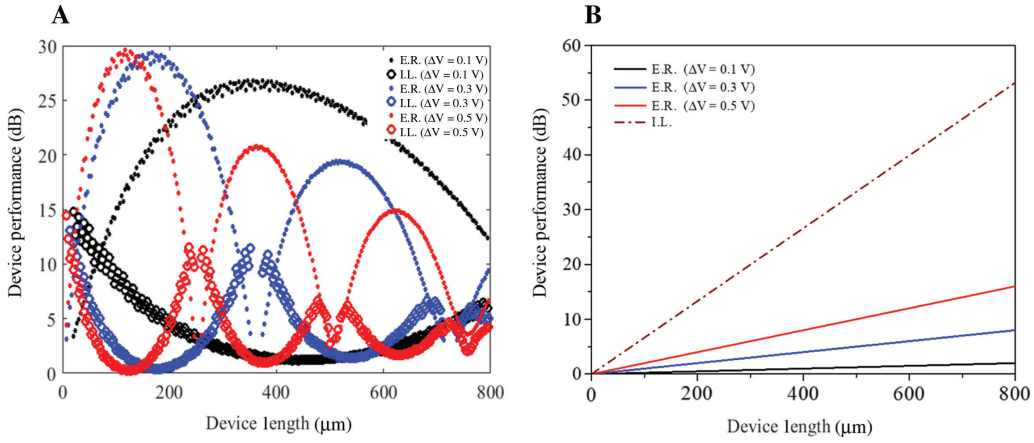

Figure 3: Extinction ratio versus insertion loss.
The evolutions of extinction ratio (solid lines) and insertion loss (dashed lines) with the device length in the ACW-ITO modulator at different bias voltages of (A) 0.1 V (black), 0.3 V (blue), 0.5 V (red). (B) Conventional ITO modulator [20] at the bias voltage of (C) 0.1 V (black), 0.3 V (blue), and 0.5 V (red). The wavelength is 1.55 μm.

utilized to terminate the 4 × 4 μm computational domain. Grid sizes of 1 and 5 nm are used to mesh ITO/Au layers and rest of the waveguide structures, respectively. The simulations are performed at a free space wavelength of $\lambda = 1.55$ μm.

2 Results

Figure 2A depicts intensity evolution in three identical waveguides, where $K_{12} = K_{23}$ and the light is injected in waveguide 1. This evolution is equivalent to on-resonant three-level atomic interactions, where all the electrons are initially in the ground state. As seen in AE conditions, the light injected in one of the outer waveguides propagates only in the other outer waveguide. The middle waveguide is effectively eliminated, as its energy build-up remains very low during the entire propagation. As seen in Figure 2B, ON-state propagation experiences less overall loss as compared to OFF state. This is due to the fact that epsilon-near-zero property of the ITO increases and consequently cancels loss of the gold. As shown in Figure 2B, even with 100 mV of peak-to-peak voltage we can see clear modulation ~440 μm device length. Insertion loss of <1.4 dB is expected from this design. Also a power consumption of 50 atto-Joule paves the path for next generation of optical interconnects.

Figure 3 shows the extinction ratio and insertion loss, respectively, based on the device length under various bias voltages in sub-volt range in the proposed ACW ITO modulator and conventional ITO modulator [20]. As shown in Figure 3 optical absorption in middle waveguide enlarges with the increase in device length and applied bias voltage. However, due to the phase detuning of the ON state from $(2N+1)\pi$ in the output port, the overlap of optical power with the center waveguide reduces with the longer device length. As a result, insertion loss for longer device length first becomes smaller and then larger. For instance, at a driving bias voltage of 0.1 V, a device length of 440.5 μm provides an insertion loss of 1.4 dB, which increases with the larger length. In contrast,

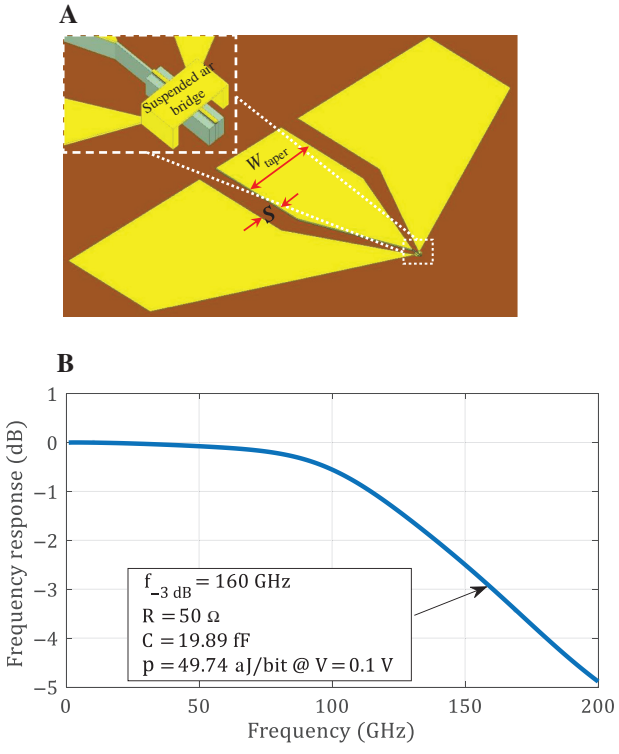

Figure 4: Limitation of modulation speed.
(A) Radio frequency (RF) pads and suspended air bridge design. (B) Frequency response of parasitic elements for RF pads and active region where $W_{taper} = 60$ μm, $S = 50$ μm, and device length is 440 μm.

Table 1: Comparison of performances between our modulator and established modulation techniques.

Structure	Principle of operation	Thermal stability (°)	Device footprint (μm^2)	Modulation depth (dB)	Insertion loss (dB)	Power consumption per bit (fJ)	Modulation speed (GHz)	Optical bandwidth (nm)
Mach-Zehnder	Depletion [23]	Good	10^4	5	2.5	3.4×10^3	18	>100
Ring-graphene	Electrical gating [7]	Very poor	6.4×10^3	10	12.5	800	30	<0.1
Disk	Reverse biased [24]	Moderate	23	8	0.92	1.03	22	<0.1
SiGe	Reverse biased [25]	Good	55	6	10	60	40.7	35
Lithium niobate	Pockels effect [26]	Very poor	6.8×10^3	18	2	1.7×10^3	20	>100
Graphene	Electrical gating [12]	Very good	18	2.1	0.9	1.4×10^3	35	>100
Plasmonic	Pockels [22]	Good	7.75×10^4	27	8	300	170	>100
Adiabatic elimination – thermal	Electrical tuning [15]	Good	200	20	2	8×10^3	0.1	>100
This work	Electrical tuning	Good	<230[a]	>25[b]	>0.25	>0.05[b]	>150	20[b]

[a]Device footprint can be traded for power consumption and modulation speed.
[b]Optical bandwidth for 20 dB extinction ratio and 0.5 dB insertion loss.

conventional ITO modulators cannot provide sub-volt operation with a reasonable insertion loss. For instance as shown in Figure 3B, even at a driving bias voltage of 0.5 V a 16 dB insertion loss is expected to obtain a 6–7 dB extinction ratio. However, as shown in Figure 3A our ACW modulator provides an extinction ratio exceeding 25 dB at a driving bias voltage as low as 0.1 V. The insertion loss changes from 1.4 to 0.25 dB, with an increase in the driving voltage from 0.1 to 0.5 V. It is noted that the conventional ITO modulator at a bias voltage of 2.5 V provides an extinction ratio of 10 dB with the insertion loss of 0.6 dB [20]. This voltage is high to perform atto-Joule modulation.

Next, we explored the limitation of the modulation speed caused by parasitic elements containing both radio frequency (RF) pads and active region. To this end, a full-wave three-dimensional simulation is performed via "Ansys Electronics Desktop". The silicon layer is considered to be doped to 10^{19} cm^{-3} levels to provide 50 Ω resistivity for the device. A Debye model is used to extrapolate frequency range of the measurement data provided in Ref. [21] for conductivity, real and imaginary part of permittivity of ITO. Next, dimensions of RF pads (W_{taper} and S in Figure 4A) are optimized for a 50 Ω and 100 μm-pitch ground-signal-ground microprobe. As shown in Figure 4A we used the suspended air bridge to connect the pad to the top gold without interfering modes of the outer waveguides [22]. The other contact is provided through the extension of the middle waveguide as shown in the inset of Figure 4A. Tapered lines are used for impedance matching of the device (50 Ω). As can be seen in Figure 4B, a modulation speed of about 160 GHz is achieved for 440 μm of the device length which is crucial for millimeter wave applications. This speed and the 50 Ω impedance of the device give us a 19.89 fF equivalent capacitance and a 49.74 aJ/bit power consumption, accordingly, at 0.1 V of modulation voltage.

Finally, Table 1 summarizes the advantages of our ACW ITO modulator by comparing it with other well-established techniques.

In conclusion, we have developed a new concept for an energy-efficient, high-speed, and low-loss ITO plasmonic modulator. The underlying operation principle is based on altering the coupling strength of an adiabatically coupled three-waveguide system. By voltage-tuning a plasmonic mode via carrier modulation of an active ITO layer of the center waveguide of the modulator, we show that tunability in and out-of an AE region in the index-design space enables dramatic modulation depth of 25 dB for just 100 mV of applied bias. The resulting 50 atto-Joule power consumption opens a new era for electro-optic modulation in silicon photonics. With the design scheme for the device length balancing the modulation depth and insertion loss by maximizing their product, the ACW modulator obtains superior performances over the current modulator techniques. The proposed modulator exemplifies the recently discussed device performance [27] paving the way for the atto-Joule's efficient, fast and low-power-consumption on-chip optoelectronic devices [28–32] enabling new functionality for photonics interconnects [33].

Acknowledgments: We are grateful for the support of the Air Force Office of Scientific Research (AFOSR) Small Business Innovation Research (SBIR) program award number FA9550-17-P-0014 under the guidance of Dr. Gernot Pomrenke.

Author contributions: H. D. and V. J. S. conceived the idea. H. D. and R. T. C. supervised this project. H. D., E. H. and

S. S. performed the theoretical analysis. F. MK. and I. Z. performed the numerical simulations. All authors wrote and discussed the manuscript.

References

[1] Jalali B, Fathpour S. Silicon photonics. J Lightwave Technol 2006;12:4600–15.

[2] Lipson M. Guiding, modulating, and emitting light on silicon–challenges and opportunities. IEEE J Lightwave Technol 2005;23:4222–38.

[3] Streshinsky M, Ding R, Liu Y, et al. Low power 50 Gb/s silicon traveling wave Mach-Zehnder modulator near 1300 nm. Opt Express 2013;21:30350–7.

[4] Ding J, Ji R, Zhang L, Yang L. Electro-optical response analysis of a 40 Gb/s silicon Mach-Zehnder optical modulator. J Lightwave Technol 2013;3114:2434–40.

[5] Choi M, Lee RK, Yariv A. Control of critical coupling in a ring resonator-fiber configuration: application to wavelength-selective switching, modulation, amplification, and oscillation. Opt Lett 2001;26:1236–8.

[6] Baba T, Akiyama S, Imai M, et al. 50-Gb/s ring-resonator-based silicon modulator. Opt Express 2013;1:11869–76.

[7] Phare CT, Daniel Lee Y-H, Cardenas J, Lipson M. Graphene electro-optic modulator with 30 GHz bandwidth. Nat Photonics 2015;9:511–4.

[8] Liu JF, Beals M, Pomerene A, et al. Waveguide integrated, ultralow-energy GeSi electro-absorption modulators. Nat Photonics 2008;2:433–7.

[9] Jongthammanurak S, Liu J, Wada K, et al. Large electro-optic effect in tensile strained Ge-on-Si films. Appl Phys Lett 2006;89:161115.

[10] Kuo Y-H, Lee YK, Ge Y, et al. Strong quantum-confined Stark effect in germanium quantum-well structures on silicon. Nature 2005;437:1334–6.

[11] Liu M, Yin X, Ulin-Avila E, et al. A graphene-based broadband optical modulator. Nature 2011;474:64–7.

[12] Dalir H, Xia Y, Wang Y, Zhang X. Athermal broadband graphene optical modulator with 35 GHz speed. ACS Photonics 2016;3:1564–8.

[13] Ma Z, Li Z, Liu K, Ye C, Sorger V. Indium-tin-oxide for high-performance electro-optic modulators. Nanophotonics 2015;4:198–213.

[14] Mrejen M, Suckowski H, Hatakeyama T, et al. Adiabatic elimination based coupling control in densely packed subwavelength waveguides. Nat Commun 2015;6:7565.

[15] Mrejen M, Suchowski H, Bachelard N, Wang Y, Zhang X. Low-loss and energy efficient modulation in silicon photonic waveguide by adiabatic elimination scheme. Appl Phys Lett 2017;111:033105.

[16] Ma Z, Tahersima MH, Khan S, Sorger VJ. Two-dimensional material-based mode confinement engineering in electro-optic modulators. IEEE J Selected Topics Quantum Electron 2017;23:1–8.

[17] Amin R, Suer C, Ma Z, Khurgin J, Agarwal R, Sorger VJ. A deterministic guide for material and mode dependence of on-chip electro-optic modulator performance. Solid-State Electron, Special Issue, 2017;136:92–101.

[18] Amin R, Suer C, Ma Z, et al. Active material, optical mode and cavity impact on electro-optic modulation performance. Nanophotonics 2018;7:455–472.

[19] Shun LC, ed. Physics of optoelectronics devices, New York, USA: Wiley-Interscience Publication, 1995:294–309.

[20] Sorger VJ, Lanzillotti-Kimura ND, Ma R-M, Zhang X. Ultra-compact silicon nanophotonic modulator with broadband response. Nanophotonics 2012;1:1–6.

[21] Alwan EA, Kiourti A, Volakis JL. Indium tin oxide film characterization at 0.1–20 GHz using coaxial probe method. IEEE Access 2015;3:648–52.

[22] Haffner C, Heni W, Fedoryshyn Y, et al. All-plasmonic Mach-Zehnder modulator enabling optical high-speed communication at the microscale. Nat Photon 2015;9:525–8.

[23] Galacho DP, Baudot C, Hirtzlin T, et al. Low voltage 25 Gbps silicon Mach-Zehnder modulator in the O-band. Opt Express 2017;25:11217–22.

[24] Timurdogan E, Sorace-Agaskar CM, Sun J, Hosseini ES, Biberman A, Watts MR. A one femtojoule athermal silicon modulator. Physics Optics arXiv:1312.2683.

[25] Feng D, Liao S, Liang H, et al. High speed GeSi electro-absorption modulator at 1550 nm wavelength on SOI waveguide. Opt Express 2012;20:22224–32.

[26] Rao A, Patil A, Rabiei P, DeSalvo R, Paolella A, Fathpour S. Lithium niobate modulators on silicon beyond 20 GHz. Proc Opt Interconnects Conf 2016, IEEE (Institute of Electrical and Electronics Engineers, 2016), Paper WC6.

[27] Liu K, Sun S, Majumdar A, Sorger VJ. Fundamental scaling laws in nanophotonics. Nat Sci Rep 2016;6:37419.

[28] Pickus SK, Khan S, Ye C, Li Z, Sorger VJ. Silicon plasmon modulators: breaking photonic limits. IEEE Photonic Soc 2013;27:6.

[29] Ye C, Liu K, Soref R, Sorger VJ. 3-Waveguide 2×2 plasmonic electro-optic switch. Nanophotonics 2015;4:261–8.

[30] Liu K, Li N, Sadana DK, Sorger VJ. Integrated nano-cavity plasmon light-sources for on-chip optical interconnects. ACS Photonics 2016;3:233–42.

[31] Li N, Liu K, Sadana DK, Sorger VJ. Nano III–V plasmonic light-sources for monolithic integration on silicon. Nat Sci Rep 2015;5:14067.

[32] Fratalocchi A, Dodson CM, Zia R, et al. Nano-optics gets practical. Nat Nanotechnol 2015;10:11–5.

[33] Sun S, Badaway A, Narayana V, El-Ghazawi T, Sorger VJ. Photonic-plasmonic hybrid interconnects: efficient links with low latency, energy and footprint. IEEE Photonics J 2015;7:6.